Power load studies in JET and ASDEX-Upgrade with full-W divertors

2013 Plasma Phys. Control. Fusion 55 124039

(http://iopscience.iop.org/0741-3335/55/12/124039)

Plasma Phys. Control. Fusion **55** (2013) 124039 (8pp) doi:10.1088/0741-3335/55/12/124039

Power load studies in JET and ASDEX-Upgrade with full-W divertors

B Sieglin[1], T Eich[1], A Scarabosio[1], G Arnoux[2], I Balboa[2], S Devaux[1], A Herrmann[1], F Hoppe[1], M Hölzl[1], A Kallenbach[1], P Lang[1], G F Matthews[2], S Marsen[3], S Pamela[2], M Rack[4], R Wenninger[1], the ASDEX Upgrade Team and JET EFDA Contributors[5]

JET-EFDA, Culham Science Centre, Abingdon, OX14 3DB, UK
[1] Max-Planck-Institute for Plasma Physics, Boltzmannstr. 2, D-85748 Garching, Germany
[2] CCFE, EURATOM-Association, Culham Science Centre, Abingdon, OX14 3DB, UK
[3] Max-Planck-Institute for Plasma Physics, Wendelsteinstr.1, 17491 Greifswald, Germany
[4] Institute of Energy and Climate Research-Plasma Physics, Forschungszentrum Jülich GmbH, Association EURATOM-FZJ, Partner in the Trilateral Euregio Cluster, D-52425 Jülich, Germany

E-mail: Bernhard.Sieglin@ipp.mpg.de

Received 4 July 2013, in final form 9 September 2013
Published 28 November 2013
Online at stacks.iop.org/PPCF/55/124039

Abstract
For the design and operation of large fusion devices, a detailed understanding of the power exhaust processes is necessary. This paper will give an overview of the current research on divertor power load mechanisms. The results shown are obtained in JET with the ITER-like wall (ILW)and ASDEX-Upgrade with tungsten coated plasma-facing components (PFCs). The challenges of infrared thermography on an ITER-like bulk tungsten divertor are presented. For the steady-state heat load, the power fall-off length λ_q in JET-ILW is compared to an empirical scaling found in JET and the ASDEX-Upgrade with carbon PFCs. A first attempt to scale the divertor broadening S in the ASDEX-Upgrade with tungsten PFCs is shown. The edge localized mode (ELM) duration t_{ELM} in JET-C and JET-ILW is compared. For similar pedestal conditions ($T_{\mathrm{e,ped}}$ and $n_{\mathrm{e,ped}}$), similar ELM durations are found in JET-C and JET-ILW. For higher $n_{\mathrm{e,ped}}$ at the same pedestal pressure $p_{\mathrm{e,ped}}$, longer ELM durations are found in JET-ILW. The pedestal pressure $p_{\mathrm{e,ped}}$ is found to be a good qualifier for the ELM energy fluency in both JET-C and JET-ILW. Improved diagnostic capabilities reveal ELM substructures on the divertor target occurring a few milliseconds before the ELM crash.

(Some figures may appear in colour only in the online journal)

1. Introduction

Control of the power exhaust in the divertor is a critical topic for present-day devices (e.g. ASDEX-Upgrade and JET) and even more for future tokamak devices, such as ITER where significantly more power enters the scrape-off layer (SOL). Quantification and interpretation of the power and energy exhaust at the divertor target plates in these present-day devices in the so-called baseline scenario, the type I ELMy H-mode, is crucial for the extrapolation to ITER. The power handling of the involved target plates is becoming more critical as plasma-facing components (PFCs) made of carbon-based materials have, in recent years, been replaced by metallic components made of tungsten. The ASDEX-Upgrade demonstrated operation with a full tungsten wall in 2007. Since 2011, JET has been equipped with the ITER-like wall (ILW) [1], with PFC made of beryllium in the main chamber and tungsten in the divertor. The exchange of the wall material was, in the first place, driven by the unacceptably high tritium retention in the presence of carbon-based PFCs. Both the ASDEX-Upgrade and the JET-ILW demonstrated a reduction of tritium retention to acceptable levels [2, 3].

[5] See the appendix of Romanelli F *et al* 2012 *Proc. 24th IAEA Fusion Energy Conf. 2012 (San Diego, CA)*.

2. Challenges of heat flux measurements on W PFCs

For typical divertor target temperatures between 300–1500 °C bulk tungsten has a low emissivity of about $\epsilon = 0.05$–0.2 at the wavelength range of 4.0–4.5 μm used for the IR measurement [4, 5]. This low emissivity leads to a low photon flux at low temperatures, where reflected light from the main chamber can influence the IR measurement. For high temperatures connected to regions with high heat loads, as observed near the strike line and during edge localized modes (ELMs),

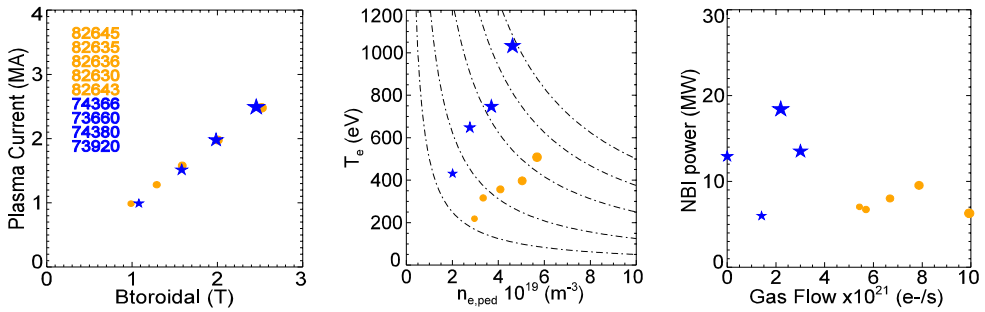

(a) Magnetic field and plasma current.

(b) Pedestal electron temperature and density.

(c) Heating power and gas fueling rate.

Figure 1. Comparison between dedicated discharges in JET-C (blue) and JET-ILW with low heating power (orange).

no significant influence (<5%) of the reflections has been estimated.

In contrast to the CFC target in JET-C, the bulk tungsten outer target plate in JET-ILW is not a uniform block, but consists of four stacks of 24 lamellae each [6]. This castellation poses a challenge on the IR measurements of the surface temperature distribution. The toroidal width of each lamella is about 6 mm, with a gap of about 1 mm in between two neighboring lamellae. The JET IR system for the outer horizontal divertor target has a spatial resolution of about 1.7 mm [5]. Therefore, an exact positioning of the measurement has to be ensured throughout the whole plasma pulse, in order to avoid a corruption of the measured surface temperature due to the influence of the toroidal gap.

During plasma operation, magnetic forces induced by the poloidal field coils and the plasma current itself cause a slight inclination (about 1 cm related to the target) of the mounting of the camera on top of the JET device. The impact of the camera movement on the measurement on the target plate has been corrected by two techniques. The first technique uses a phase correlation method to calculate the movement of the camera directly from the measured data. For the second technique, the movement in different test pulses with and without plasma and different poloidal field currents were analyzed using the first technique. The results were used to calculate the movement based on the plasma and various coil currents. This method has been validated using discharges with different plasma scenarios, where the IR measurement allowed the application of the first technique. An accuracy of about 0.5 mm (∼1/4 pixel) was reached. These techniques were used for the IR measurements during the 2011–2012 campaign in the JET-ILW. For castellated structures, as foreseen in ITER, those methods are thought to be a valuable tool for IR thermography.

3. Dedicated discharges

To obtain optimal IR measurements, dedicated discharges have been conducted in JET-ILW.

Figure 1 shows the obtained plasma conditions for a scan in magnetic field B_t and plasma current I_p in JET-ILW with low heating power $P_{heat} < 10$ MW. The reference discharges from JET-C are shown in blue. JET-ILW operated at a higher gas flow ($\Gamma_D = (5–10) \times 10^{21}\,s^{-1}$) compared to JET-C ($\Gamma_D = (0–3) \times 10^{21}\,s^{-1}$) to prevent impurity accumulation [7, 8] (figure 1(*c*)). The higher gas flux and the slightly lower heating power in JET-ILW lead to a different pedestal composition [9]. The achieved pedestal electron density is higher and the pedestal electron temperature is lower (figure 1(*b*)). Comparable discharges were carried out at the last phase of JET-C operation with the outer target plate of the same geometry made by CFC.

In a second attempt, discharges at a higher auxiliary neutral beam heating power of up to 26 MW have been executed in order to recover the pedestal temperatures observed in JET-C with the JET-ILW (figure 2(*c*)). For these discharges, similar pedestal conditions to the ones in JET-C have been reached (figure 2(*b*)).

4. Steady-state heat load

In this section, the steady-state heat flux pattern at the outer divertor target is characterized. This applies to L-mode and inter-ELM phases in H-mode. For the target heat flux distribution, a model was presented in [10].

$$q(\bar{s}) = \frac{q_0}{2} \exp\left(\left(\frac{S}{2\lambda_q}\right)^2 - \frac{\bar{s}}{\lambda_q f_x}\right) \operatorname{erfc}\left(\frac{S}{2\lambda_q} - \frac{\bar{s}}{S f_x}\right), \quad (1)$$

where λ_q is the power fall-off length, S is the divertor broadening, $\bar{s}$ is the target position relative to the strike line, q_0 is the peak heat flux density at the divertor entrance and f_x is the flux expansion for the given magnetic configuration.

Figure 3 shows the measured divertor broadening and power fall-off length for the ASDEX-Upgrade (Divertor I and IIb [11, 12]) with carbon PFCs, JET-C and JET-ILW [13]. For the dedicated discharges, no difference in the steady-state heat load on the target plates is observed, when comparing JET-C and JET-ILW. The data from the ASDEX-Upgrade shows a large difference in the measured divertor broadening S, dependent on the divertor configuration. Divertor I, which is an open configuration, has an average value of $S = 0.4$ mm and the closed divertor IIb has an S of about 1.6 mm.

4.1. Power fall-off length λ_q

As a first step, an attempt was made to validate the empirical inter-ELM H-Mode scaling for the power fall-off length λ_q

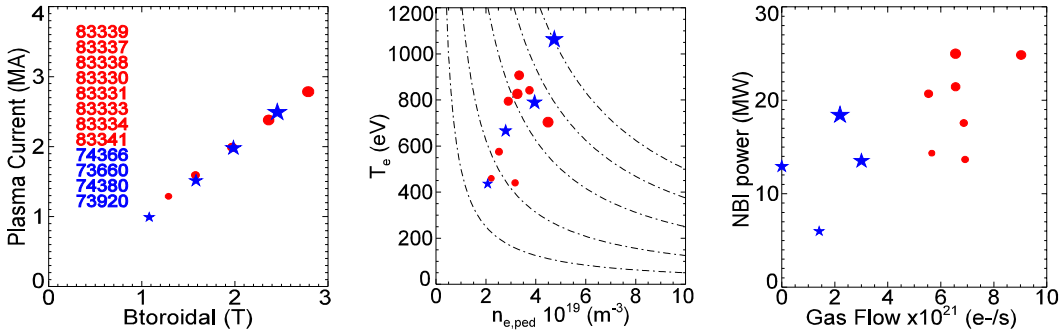

(a) Magnetic field and plasma current.

(b) Pedestal electron temperature and density.

(c) Heating power and gas fueling rate.

Figure 2. Comparison between dedicated discharges in JET-C (blue) and JET-ILW with high heating power (red).

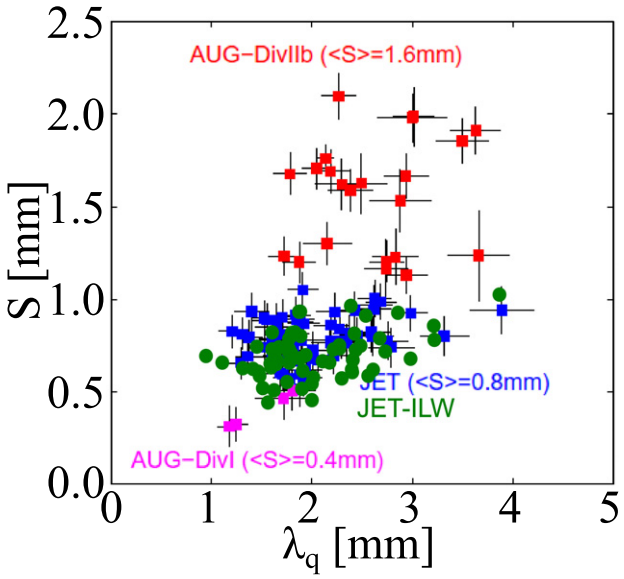

Figure 3. Divertor broadening S and power fall-off length in H-Mode for the ASDEX-Upgrade (Divertor I (magenta) and divertor IIb (red)), JET-C (blue) and JET-ILW (green).

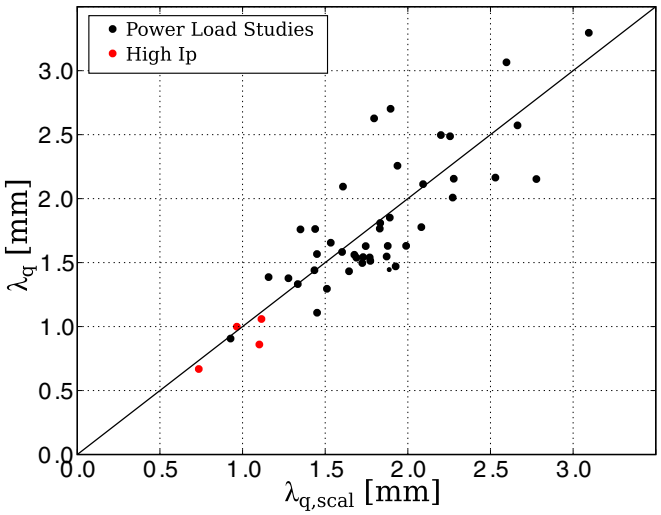

Figure 4. Comparison of the measured power fall-off length λ_q in JET-ILW with the empirical scaling obtained in JET and ASDEX-Upgrade with carbon PFCs (equation (2)).

(equation (2)) [13], resulting from the JET and ASDEX-Upgrade data with carbon PFCs, in the JET-ILW.

$$\lambda_{q,\mathrm{scal}}[\mathrm{mm}] \widehat{=} 0.73\, B_{\mathrm{t}}^{-0.8}\, q_{\mathrm{cyl}}^{1.2}\, P_{\mathrm{SOL}}^{0.1}\, R^{0.0}. \qquad (2)$$

Figure 4 shows the measured power fall-off length λ_q in the JET-ILW compared to the empirical scaling in different operational regimes up to a toroidal magnetic field of 3.5 T and a plasma current of 3.5 MA. It is found that the power fall-off length in the JET-ILW for attached divertor conditions can be described by the empirical scaling (2) found in carbon ASDEX-Upgrade and JET-C.

4.2. Divertor broadening S

One important quantity for the assessment of the divertor power load in a tokamak is the integral power fall-off length λ_{int}:

$$\lambda_{\mathrm{int}} = \frac{1}{q_{\mathrm{max}}} \int q(s)\, \mathrm{d}s, \qquad (3)$$

where q_{max} is the peak heat flux on the target.

Using (1), a simple relation between λ_{int} and both the power fall-off length λ_q and the divertor broadening S can be derived, as shown by Makowski [14]:

$$\lambda_{\mathrm{int}} \approx \lambda_q + 1.64\, S, \qquad (4)$$

with this, it becomes clear that an understanding of the divertor broadening S is mandatory to be able to estimate λ_{int}. For large values, S can be the dominant contribution to λ_{int}, compensating for a small λ_q. In order to get well defined experimental and divertor conditions, dedicated L-Mode discharges with low recycling divertor conditions have been conducted in the ASDEX-Upgrade in deuterium and hydrogen. For the scaling of S, different quantities, such as the pedestal electron density $n_{\mathrm{e,ped}}$, the neutral gas density in the divertor $n_{0,\mathrm{div}}$, the specific isotope mass A and the poloidal magnetic field B_{pol}, have been examined. The best match of the measured divertor broadening, with a residual sum of squares of 0.93, has been found with the following relation (figure 5):

$$S[\mathrm{mm}] \widehat{=} (0.09 \pm 0.01)\, n_{\mathrm{e,ped}}^{1.02\pm0.03}\, B_{\mathrm{pol}}^{-1.01\pm0.05}, \qquad (5)$$

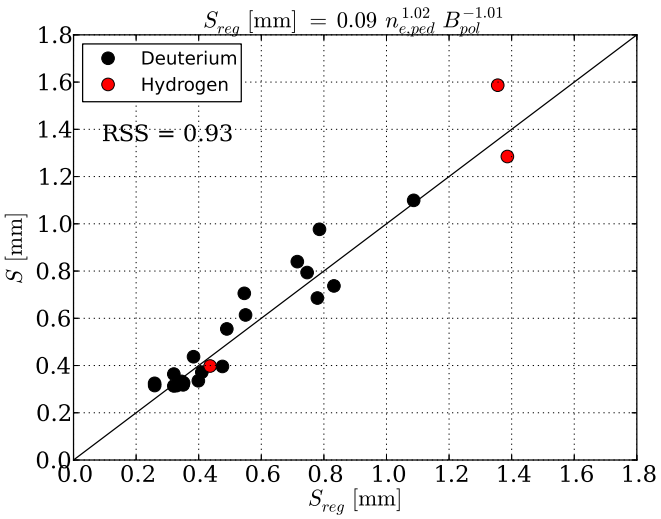

Figure 5. Regression results of the measured divertor broadening S in ASDEX-Upgrade L-Mode discharges.

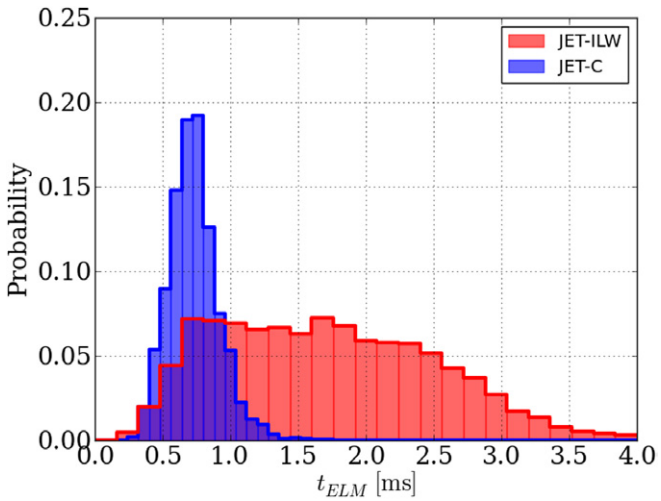

Figure 6. Comparison of the ELM duration t_{ELM} for JET-C and JET-ILW for type I ELMy H-modes ($f_{\mathrm{ELM}} < 100$ Hz).

where $n_{\mathrm{e,ped}}$ is the pedestal electron density in $10^{19}\,\mathrm{m}^{-3}$ and B_{pol} is the poloidal magnetic field in T:

$$B_{\mathrm{pol}} = \frac{\mu_0\, I_{\mathrm{p}}}{2\,\pi\, a}\left(\frac{1+\kappa^2}{2}\right)^{-0.5}, \qquad (6)$$

with the plasma current I_{p}, the minor radius a and the elongation κ. So far no isotope dependence of the divertor broadening S has been observed. We note here that no dependence of S on the neutral gas density $n_{0,\mathrm{div}}$ has been found. For the investigation of the dependence of the divertor broadening on the machine size, the same study has to be performed in JET. This, however, is an ongoing process and cannot be shown in this work.

5. ELM induced transient heat load

In H-Mode, periodic ELMs induce high transient heat loads onto the divertor target plates. In contrast to the very localized steady state heat flux, the ELM heat load is unevenly deposited onto a comparable large area. For the measurement of the impact on the divertor target, the deposited energy fluency ϵ in kJ m^{-2} is taken. In the dedicated discharges, the strike line position was set to ensure that the maximum of the energy fluency is within the observed area.

In devices with carbon PFCs, the deposition of hydrocarbon layers can corrupt the measurements, resulting in an overestimation of the peak heat flux [15]. In the JET-ILW, no formation of deposition layers (e.g. beryllium) has been observed, which has an impact on the analysis on the outer horizontal target over the whole campaign.

For the estimation of the divertor target lifetime, an important quantity is the heat impact factor $P\sqrt{t_{\mathrm{ELM}}}$ [16]:

$$P\sqrt{t_{\mathrm{ELM}}} = \frac{\epsilon_{\mathrm{ELM}}}{\sqrt{t_{\mathrm{ELM}}}} = \frac{E_{\mathrm{ELM}}}{A_{\mathrm{wet}}}\frac{1}{\sqrt{t_{\mathrm{c}}}}, \qquad (7)$$

where ϵ_{ELM} is the deposited energy fluency and t_{ELM} is the energy deposition time. For an acceptable lifetime of the ITER divertor, a limit of 500 kJ m^{-2} is found by material testing for a typical energy deposition time of 750 μs [16, 17].

5.1. ELM duration t_{ELM}

The first critical value for the impact of the ELM on the divertor target is the ELM duration t_{ELM}, in which the ELM deposits its energy on the target. The pedestal electron temperatures and densities reached in JET-C (blue) and JET-ILW (red) are shown in figure 7(a) for the discharges used in the comparison. The distribution of the ELM duration found in JET-C and JET-ILW are shown in figure 6. In the JET-C, an average value of about 750 μs is found and the variance in the ELM duration is small. In the JET-ILW, the average ELM duration is longer (about 2 ms) and the distribution is wider. However, the shortest ELMs reach the values observed in the JET-C.

In figure 7(a), the electron temperature and densities are shown for a set of discharges in type I ELMy H-mode in the JET-C and the JET-ILW. The JET-ILW typically operates at a higher density for a given pedestal pressure, in comparison with the JET-C. As shown in figure 7(b), the ELM durations for the same pedestal conditions in the JET-C (blue) and the JET-ILW (green) are comparable. For a higher density at the same pedestal pressure (orange) in the JET-ILW, the ELM duration becomes longer and the width of the distribution increases.

This observation shows that the ELM induced divertor heat load characteristic in the JET-ILW is not largely different to in the JET-C. The dedicated discharges in the JET-ILW were conducted at an on average higher gas fueling rate as compared to the JET-C, leading to plasma conditions which exhibit longer ELM durations.

5.2. ELM energy fluency ϵ_{max}

In the following, the ELM energy fluency in JET-ILW and JET-C are compared. The energy fluency is calculated by integrating the heat flux $q(s,t)$ over the ELM duration:

$$\epsilon(s) = \int_{\mathrm{ELM}} q(s,t)\,\mathrm{d}t. \qquad (8)$$

Figure 8 shows an example of the ELM target heat load footprint and the resulting energy fluency profile. For the

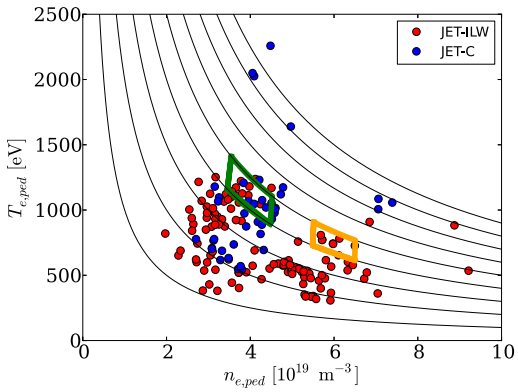

(a) Pedestal temperatures and densities for JET-C and JET-ILW with lines of constant pressure (black). Boxes show The operational space used for the comparison of the ELM duration for low (green) and high (density) at constant pedestal pressure.

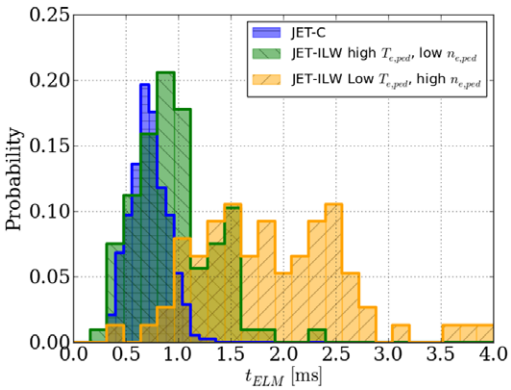

(b) ELM duration in JET-ILW at constant pressure but different pedestal composition ($n_{e,ped}/T_{e,ped}$).

Figure 7. Comparison of ELM duration in ILW at different pedestal conditions.

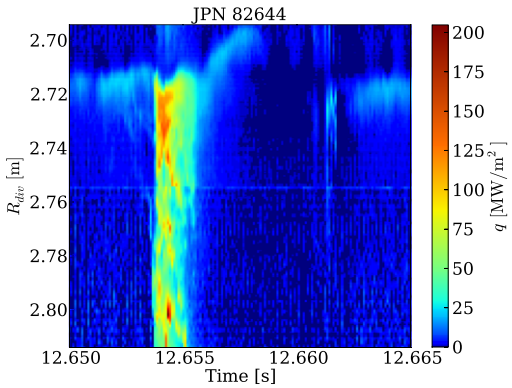

(a) ELM target heat load foot print in JET-ILW.

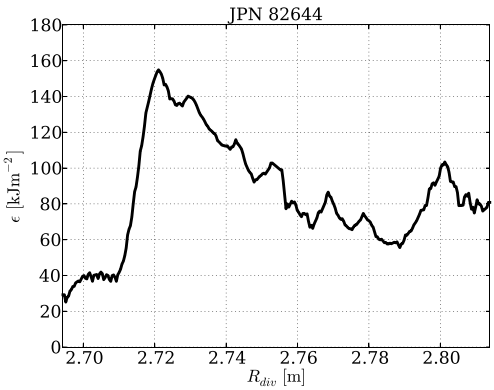

(b) Target ELM energy fluency profile.

Figure 8. Target heat load footprint and energy fluency for a Type-I ELM in JET-ILW.

comparison of the ELM induced power load in the JET-C and the JET-ILW, the peak energy fluency $\epsilon_{\max}$ is used.

$$\epsilon_{\max} = \max\left(\epsilon(s)\right). \tag{9}$$

In order to account for the different magnetic inclination angles in the JET-C and the JET-ILW [18], the parallel energy fluency is calculated. Figure 9 shows the parallel peak energy fluency $\epsilon_{||,\max}$ for the JET-C and the JET-ILW plotted against the pedestal electron pressure $p_{\mathrm{e,ped}}$. It can be seen that the energy fluency for both the JET-C and the JET-ILW are within experimental scatter, the same as for the same pedestal pressure. Whether the linear relation between the peak energy fluency and the pedestal pressure is valid for higher pressure cannot be answered here. However, the existing data indicates that this relations forms an upper limit for the deposited peak energy fluency.

6. ELM substructure

An ELM is understood as a magnetohydrodynamic (MHD) mode in the plasma edge that is identified as a peeling–ballooning mode [19]. Once an ELM becomes non-linearly unstable, it causes an out-flux of particles from the plasma edge into the SOL [20]. This comes along with a strong drop of the electron pedestal temperature and density. One part of the energy that leaves the confined plasma is radiated, another part is deposited as heat on the target plates in the divertor region. The ELM duration on the divertor target is set by the energy efflux time and the SOL transport time. The SOL transport time is described by a free-streaming process of the particles that are ejected from the confined plasma region into the SOL [21]. Typical rise times for the heat load on the target plates are in the order of a few hundred microseconds [4]. The energy efflux time is a result of a complex non-linear process, possibly including the interaction with SOL currents [22].

The heat load deposited during an ELM crash shows a characteristic pattern. An ELM causes a natural ergodization of the plasma edge [23], which results in a random deposition of the heat load on the target plates, i.e. each ELM crash appears different. However, typical features have been observed, like a radial decay of the deposited energy on the target in the outward direction and filamentary structures that appear during

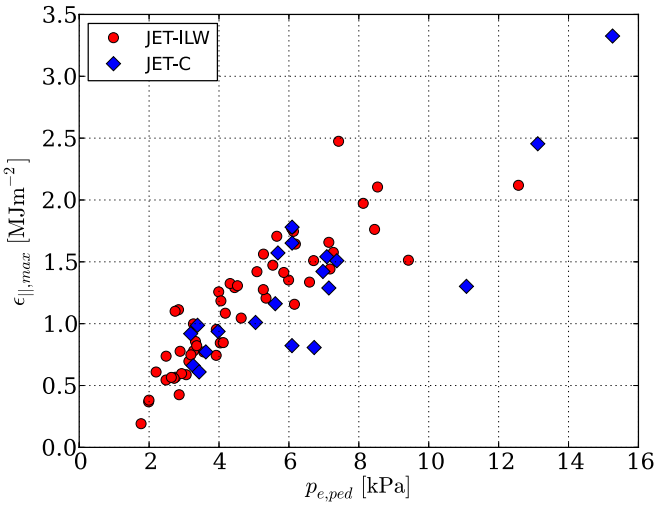

Figure 9. Parallel peak energy fluency $\epsilon_{||,\max}$ and pedestal electron pressure $p_{\mathrm{e,ped}}$ for JET-C (blue) and JET-ILW (red).

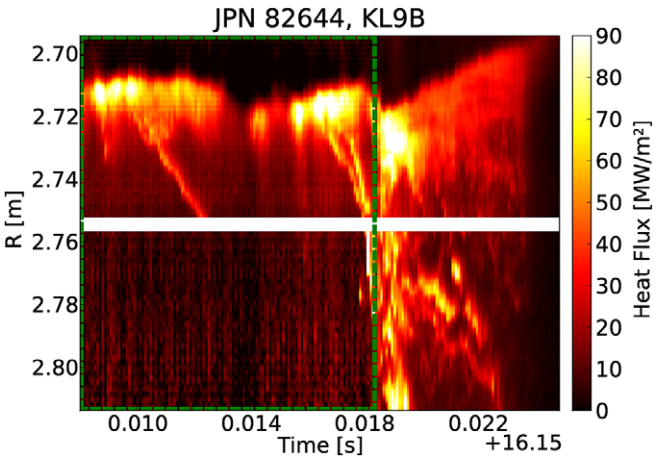

Figure 10. Heat load deposition pattern of one ELM for discharge with JET pulse number (JPN) 82644. The dashed rectangle marks a region where the heat load is magnified by a factor of five for an easier visibility of the pre-ELM structures.

the ELM crash. The number of filamentary structures increases during the ELM crash and a quasi-toroidal mode number is defined for ELMs [24, 25]. In the early phase of an ELM crash, a low mode number, $n = 3$ to 5, is identified, which increases to about $n = 10$ to 20 during the ELM crash.

ELMs are associated with toroidally rotating filaments [26]. These filaments are created in the plasma edge and leave the confined region during the ELM crash. A radial propagation speed of the ELM filament in the range of 0.5 to 2 km s^{-1} is found [27]. For a typical JET plasma shape, the radial spacing between the wall and the plasma is around 6–7 cm at the outer mid-plane. From this, we can calculate the time an ELM filament spends in the SOL before interacting with the wall and collapsing to be in the range of a hundred microseconds, which corresponds to the ELM crash rise time seen in the divertor heat load. The filamentary structures in the heat load have been linked to the appearance of ELM filaments and modeled with a reduced non-linear MHD code [28]. The modeling results show that these filamentary structures can be understood as poloidally rotating ballooning modes.

Recent experiments on the JET-ILW [1] have shown the occurrence of radial propagating structures in the divertor heat load prior to the ELM crash, see figure 10. These pre-ELM structures have a lifetime of several milliseconds and can therefore not be caused by the faster radial propagating ELM filaments that were discussed before. A few milliseconds before the ELM crash, a small increase of the heat flux on the original strike line position is seen. At that time, the radial outward propagating structures are created at the same location. The pre-ELM structures propagate with a radial speed of around 10 to 20 m s^{-1} and continue until the larger main ELM crash heat deposition pattern. The heat deposition pattern of the ELM crash appears to be influenced by the structures, as stronger heat fluxes are measured at those positions where the structures connect to the pattern. After the ELM crash, the structures vanish. The white line in figure 10 marks the gap between the two stacks of the Tungsten divertor. Some pre-ELM structures seems to stop at that gap, see 8 ms before the ELM crash in figure 10. This either means that those pre-ELM structures do not necessary lead to an ELM crash, or that they do not reach the target plates because of the poloidal shadowing of the different stacks. In the given example, the very early pre-ELM structure is not seen on the outer stack ($R \approx 2.757$ cm to 2.814 cm), but during the ELM crash, an increased heat flux is seen at the position where this structure would have ended ($R \approx 2.81$ cm) if it continued with the same speed. These substructures are visible in most of the discharges in the JET-ILW. An attempt was made to study these pre-ELM structures in the JET-C and there the structures develop very quick. The temporal resolution of the IR system is not sufficient to resolve the structures in the JET-C.

The pre-ELM structures are created before the ELM crash, i.e. before the large amount of energy and particles is lost into the SOL. Furthermore, the structures appear as several parallel stripes. This is similar to the strike line splitting known from the effects of magnetic perturbations on low-confinement mode plasmas [29]. While ELM filaments cannot explain the observations, a possible explanation is an early change of the magnetic topology, several milliseconds before the ELM. This indicates that processes early in the ELM cycle lead to a perturbation of the plasma that finally influence the ELM crash heat deposition. During the ELM crash, the quasi-toroidal mode numbers are seen to increase from $n = 3$ to 5. The pre-ELM structures start with a single propagating stripe that increase in number until the ELM crash. The increase of stripes corresponds to an increasing quasi-toroidal mode number for the pre-ELM structures and links to the mode numbers during the ELM crash. The understanding of such an observation is of high interest in terms of ELM control. By knowing the physics of an ELM trigger, the techniques for ELM control could be optimized.

7. Summary

In this paper, an overview of current research activities of the divertor power load in JET and the ASDEX-Upgrade has been given. The challenges of IR thermography on castellated bulk

tungsten have been discussed briefly. The main conclusions to be drawn from this paper are the following.

- Despite the change in the operational space in the JET-ILW compared to the JET-C, no change in the inter-ELM power fall-off length λ_q and the divertor broadening S has been observed.
- Using dedicated low recycling L-Mode discharges in the ASDEX-Upgrade, a scaling for the divertor broadening S based on the pedestal top electron density $n_{e,ped}$ and the poloidal magnetic field B_{pol} has been found. Speculating on an absence of a size dependence in the scaling and taking values foreseen for ITER, the scaling delivers a divertor broadening S for attached conditions, which lies in the same range as observed in ASDEX-Upgrade and JET.
- In the JET-ILW, on average longer ELM durations (about 2 ms) as compared to the JET-C (about 750 μs) are found due to the on average higher pedestal densities.
- For both the JET-ILW and the JET-C, the pedestal electron pressure is found to order the parallel peak energy fluency $\epsilon_{||,max}$ deposited on the target. Thus within the experimental scatter, no difference for $\epsilon_{||,max}$ between the JET-C and the JET-ILW has been found.
- Independent of the on average longer ELM duration in the JET-ILW, no difference in $\epsilon_{||,max}$ was observed.
- Filamentary pre-ELM structures have been observed on the outer divertor target several ms before the ELM crash, giving new input for the understanding of the physics triggering an ELM. Similar features have been observed in the ASDEX-Upgrade using magnetic probes [24].

In summary, we note that tokamak operation in tungsten and CFC shows no significant difference in terms of divertor power load. Operation at higher pedestal density, as found in the JET-ILW with higher gas flow when compared to the JET-C, shows a beneficial effect due to the longer ELM time scale. Whether the ITER with a tungsten divertor will have pedestal conditions which will foster longer ELMs is yet unclear. Further studies on the role of the pedestal conditions on the ELM duration need to be conducted in both JET and the ASDEX-Upgrade.

Acknowledgments

This work was supported by EURATOM and carried out within the framework of the European Fusion Development Agreement. The views and opinions expressed herein do not necessarily reflect those of the European Commission.

References

[1] Philipps V, Mertens Ph, Matthews G F and Maier H 2010 Overview of the JET ITER-like wall project *Fusion Eng. Des.* **85** 1581–6

[2] Mayer M *et al* 2009 Carbon balance and deuterium inventory from a carbon dominated to a full tungsten ASDEX Upgrade *J. Nucl. Mater.* **390–391** 538–43

[3] Brezinsek S *et al* 2013 Residual carbon content in the initial ITER-like wall experiments at JET *J. Nucl. Mater.* **438** (Suppl.(0)) S303–8

[4] Eich T, Thomsen H, Fundamenski W, Arnoux G, Brezinsek S, Devaux S, Herrmann A, Jachmich S and Rapp J 2011 Type-I ELM power deposition profile width and temporal shape in JET *J. Nucl. Mater.* **415** (Suppl.) S856–9

[5] Balboa I *et al* and JET EFDA Contributors 2012 Upgrade of the infrared camera diagnostics for the JET ITER-like wall divertor *Rev. Sci. Instrum.* **83** 10D530

[6] Mertens Ph, Hirai T, Linke J, Neubauer O, Pintsuk G, Philipps V, Sadakov S, Samm U and Schweer B 2007 Conceptual design for a bulk tungsten divertor tile in JET *Fusion Eng. Des.* **82** 1833–8

[7] Neu R *et al* 2013 First operation with the JET International Thermonuclear Experimental Reactor-like wall *Phys. Plasmas* **20** 1–7

[8] Puetterich T *et al* 2013 the ASDEX Upgrade Team and JET EFDA Contributors 2013 Taming tungsten in JET and ASDEX Upgrade *Plasma Phys. Control. Fusion* **55** 124036

[9] Beurskens M N A *et al* 2013 the ASDEX Upgrade Team and JET-EFDA Contributors 2013 The effect of a metal wall on confinement in JET and ASDEX Upgrade *Plasma Phys. Control. Fusion* **55** 124043

[10] Eich T, Sieglin B, Scarabosio A, Fundamenski W, Goldston R J and Herrmann A 2011 Inter-elm power decay length for JET and ASDEX Upgrade: measurement and comparison with heuristic drift-based model *Phys. Rev. Lett.* **107** 1–4

[11] Kallenbach A *et al*, the ASDEX Upgrade Team and the JET Team 1999 Closed divertor operation in ASDEX Upgrade and JET *Plasma Phys. Control. Fusion* **41** B177

[12] Neu R *et al* and the ASDEX Upgrade Team 2002 Properties of the new divertor IIb in ASDEX Upgrade *Plasma Phys. Control. Fusion* **44** 1021

[13] Eich T, Sieglin B, Scarabosio A, Herrmann A, Kallenbach A, Matthews G F, Jachmich S, Brezinsek S, Rack M and Goldston R J 2013 Empiricial scaling of inter-ELM power widths in ASDEX Upgrade and JET *J. Nucl. Mater.* **438** S72–7

[14] Makowski M A, Elder D, Gray T K, Labombard B, Lasnier C J, Leonard A W, Maingi R, Osborne T H, Stangeby P C, Terry J L and Watkins J 2012 Analysis of a multi-machine database on divertor heat fluxes *Phys. Plasmas* **19** 1–9

[15] Devaux S, Arnoux G, Eich T, Thomsen H, Brezinsek S, Coad P, Likonen J, Stamp M and Widdowson A 2011 Surface layers effect on heat loads on the JET divertor targets *38th EPS Conf. on Plasma Physics 2011 (Strasbourg)* vol 35 (ECA) pp 49–52

[16] Linke J, Escourbiac F, Mazul I V, Nygren R, Rödig M, Schlosser J and Suzuki S 2007 High heat flux testing of plasma facing materials and components—status and perspectives for ITER related activities *J. Nucl. Mater.* **367–370** B(SPEC. ISS.) 1422–31

[17] Loewenhoff Th, Linke J, Pintsuk G and Thomser C 2012 Tungsten and cfc degradation under combined high cycle transient and steady state heat loads *Fusion Eng. Des.* **87** 1201–5

[18] Marsen S, Eich T, Groth M, Jachmich S and Sieglin B 2013 Experimental sheath heat transmission factors in diverted plasmas in JET *J. Nucl. Mater.* **438** (Suppl.(0)) S393–6

[19] Connor J W 1998 Edge-localized modes—physics and theory *Plasma Phys. Control. Fusion* **40** 531

[20] Wilson H R and Cowley S C 2004 Theory for explosive ideal magnetohydrodynamic instabilities in plasmas *Phys. Rev. Lett.* **92** 175006

[21] Eich T, Kallenbach A, Fundamenski W, Herrmann A and Naulin V 2009 On the asymmetries of elm divertor power

deposition in JET and ASDEX Upgrade *J. Nucl. Mater.* **390–391** 760–3

[22] Evans T E, Yu J H, Jakubowski M W, Schmitz O, Watkins J G and Moyer R A 2009 A conceptual model of the magnetic topology and nonlinear dynamics of elms *J. Nucl. Mater.* **390–391** 789–92

[23] Eich T, Herrmann A and Neuhauser J 2003 Nonaxisymmetric energy deposition pattern on ASDEX Upgrade divertor target plates during type-I edge-localized modes *Phys. Rev. Lett.* **91** 195003

[24] Eich T *et al* 2005 Type-I ELM substructure on the divertor target plates in ASDEX Upgrade *Plasma Phys. Control. Fusion* **47** 815–42

[25] Devaux S, Eich T, Arnoux G, Fundamenski W and Thomsen H 2011 Type-I ELM filamentary substructure on the JET divertor target *J. Nucl. Mater.* **415** (1, Suppl.) S865–8

[26] Kirk A, Koch B, Scannell R, Wilson H R, Counsell G, Dowling J, Herrmann A, Martin R and Walsh M 2006 Evolution of filament structures during edge-localized modes in the mast tokamak *Phys. Rev. Lett.* **96** 185001

[27] Kirk A, Lisgo S, Nardon E, Eich T, Herrmann A, Kallenbach A and Loarte A 2009 Physics of elm power fluxes to plasma facing components and implications for ITER *J. Nucl. Mater.* **390-391** 727–32

[28] Pamela S J P, Huysmans G T A, Beurskens M N A, Devaux S, Eich T, Benkadda S and JET EFDA contributors 2011 Nonlinear mhd simulations of edge-localized-modes in JET *Plasma Phys. Control. Fusion* **53** 054014

[29] Harting D M, Liang Y, Jachmich S, Koslowski R, Arnoux G, Devaux S, Eich T, Nardon E, Reiter D, Thomsen H and JET EFDA contributors 2012 Strike point splitting in the heat and particle flux profiles compared with the edge magnetic topology in a $n = 2$ resonant magnetic perturbation field at JET *Nucl. Fusion* **52** 054009